This ECT sensor is modelled using ANSYS. The conductive electrodes are taken as copper while the material for nonconductive material is taken as PVC. The ECT sensor is modelled in the electric mode. Properties of the materials used and the dimensions of sensor are defined for its geometric modelling. By setting element attribute pointers, the element attributes to the solid model entities are allocated. A mesh control is chosen and the entire structure is meshed. Meshing is used for getting finite elements which defines the accuracy of the solution obtained. Simultaneous set of equations are solved that the finite element method generates for the model. Loads are applied as electric boundary voltage on areas. The source electrode is supplied 20 V and subsequent electrodes are detector electrodes and are given 0 V one after another and results are plotted in post processing. Post processors help to find out whether the design really works when put to use. Voltage distribution is thus plotted and observed for various media. The image of every step in modelling a sensor is shown step by step in **Figure 3**.

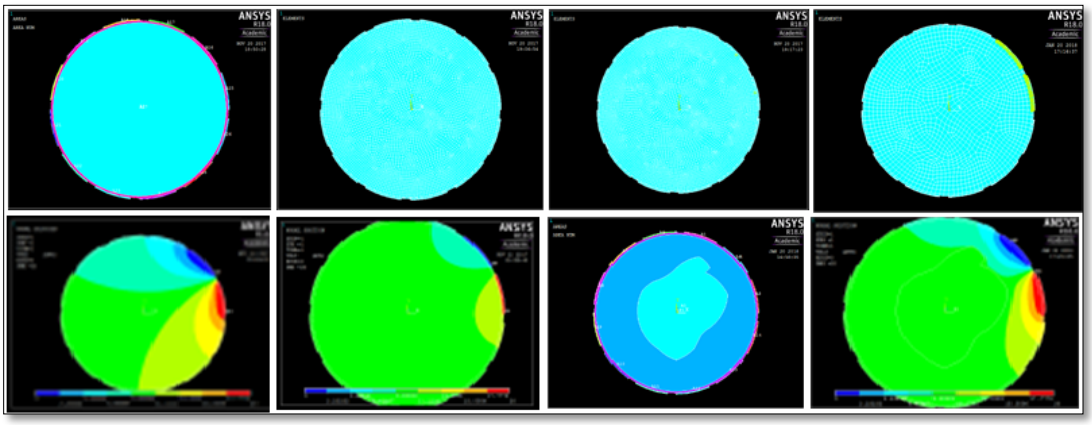

Figure 3. ECT model steps and voltage distribution for various media.

The voltage distribution within the sensor is plotted for air and water. A bone with surrounding medium as air is modelled within a sensor. The voltage distribution within the sensor with bone is plotted.

3D model of the sensor with bone within it surrounded by air is modelled and shown in **Figure 4**.

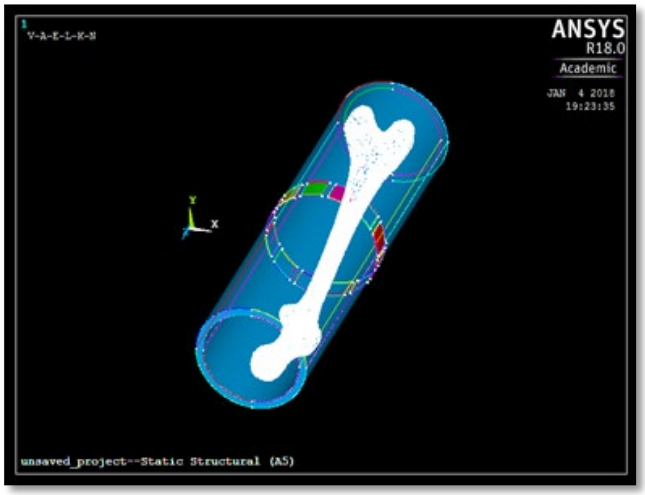

Figure 4. 3D model of sensor with bone in it.

Front view of the 3D sensor modelled is shown in **Figure 4** which is similar to the images shown in **Figure 5**.

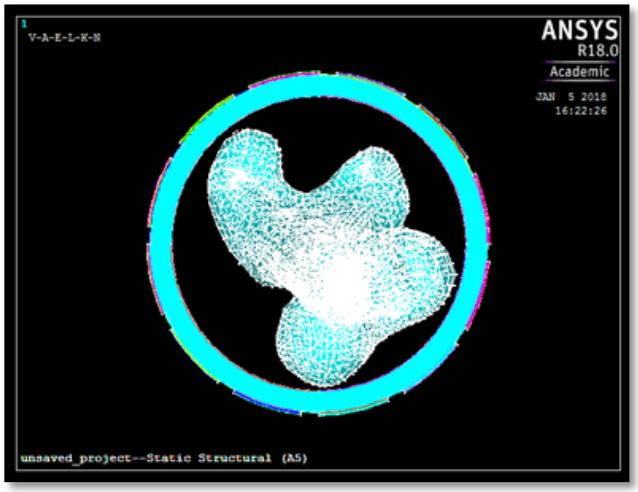

Figure 5. Front view of the 3D sensor with bone in it.

Hardware section

A 12 electrode ECT sensor is fabricated and a femur bone was sculpted according to the 3D model shown in **Figure 6**. Based on the dimensions used in the 3D model, PVC tube is used and Copper electrodes are cut out from a thin Copper sheet and fixed on the PVC tube with equal spacing using Araldite as shown in **Figure 6**. The sculpted is bone and eventually placed in the sensor as shown in **Figure 6**, to take readings of the sensor with bone in it.

Figure 6. ECT sensor, Femur bone and ECT sensor with bone placed within it.

Source of 20 V, 20 kHz square wave signal with 50% duty cycle is given by function generator to the source electrode. The current flow is measured using a multimeter by connecting it to the detector electrode. The negative terminals of function generator and multimeter are connected together thereby completing the circuit. The setup is show in **Figure 7**.

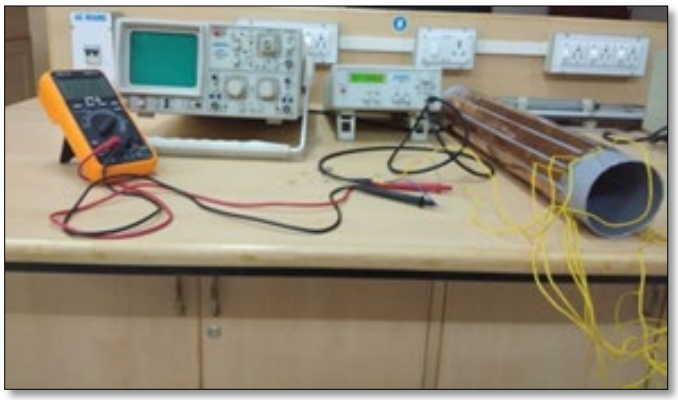

Figure 7. Hardware setup.

Signal converter

Capacitance values from sensor have to be converted to voltage values in order to be given for image reconstruction. The converter circuit is connected to a PC and the result is displayed using MATLAB. The signal converter circuit is implemented using MULTISIM. MULTISIM is a powerful schematic capture and simulate software using which electronic circuits and SPICE can be simulated and Printed Circuit Boards can be prototyped. The signal converter used here is a capacitance to voltage converter as shown in **Figure 8**.

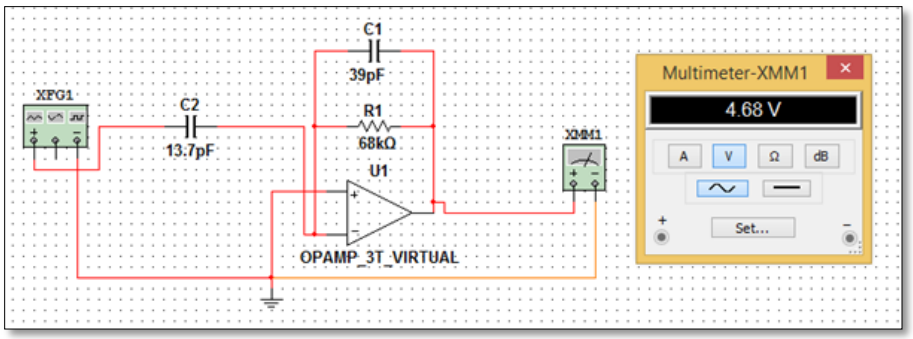

Figure 8. Capacitance to voltage converter.

The op-amp used in the circuit is a simplified 3-terminal op-amp. C_f and R_f are the feedback components. Signal generator gives a 20 V, 20 kHz source signal. In the circuit, the square wave excitation signal is generated by the signal generator which is set to 20 V amplitude and 20 kHz frequency. The excitation signal is applied to the source electrode while the detector electrode is given to negative of op-amp for that particular pair of electrodes across which the measurement is taken. The charging voltage is detected by the op amp with capacitive and resistive feedback circuits. The AC signal from the measured capacitance from ANSYS is further given for conditioning which is defined in the circuit as the known capacitance C_2. The current flowing out of C_2 is given to the I to V converter which consists of op-amp C_f, R_f which converts it into AC voltage which is measured using multimeter. The negative terminals of signal generator and multimeter are grounded and the positive terminal of the op-amp is grounded with these too. AC voltage output of the capacitance to voltage converter is directly proportional to the measured capacitance. R_f and C_f are varied to get the voltages within a particular range. The output of the capacitance to voltage is given by Equation (1).

$$V_0 = \frac{-j\omega C1Rf}{j\omega CfRf+1} V_i \qquad (1)$$

The circuit possesses features which make it suitable for biomedical application. It has the following advantages: (1) reduces drift problem, (2) provides high SNR, (3) provides good linearity and (4) immune to stray capacitances introduced by the coaxial cables and disadvantage that it can be used only for low range excitation source and will be affected by high frequency range. As the excitation voltage used is low range in order to be non-invasive for biomedical application, this signal conditioning unit is apt to be used here.

Image reconstruction

The voltage values obtained from signal conditioning unit is converted to pixel values for forming an image according to an algorithm best suited for the application. The limited voltage values which are 66 in number have to be projected onto a 32 × 32 square pixel grid within which the sensor cross section is defined. For a circular ECT sensor, the cross section is a circle with 812 pixels out of the total 1024 pixels. ECT is an inverse problem as the inter-electrode capacitances are measured while the permittivity distribution within the sensor is to be known which the inverse of the actual measurement is. The equation of the forward or actual measurement is represented in Equation (2).

$$C = S.K \qquad (2)$$

Image reconstruction algorithm is chosen based on the ease to generate it, image resolution and speed required. The principle of Linear Back Projection algorithm (LBP) is that once the set of inter-electrode capacitances C have been measured, the permittivity distribution K can be obtained from these measurements using an inverse transform Q as follows:

$$K = Q.C \qquad (3)$$

Q is the inverse of the matrix S. However, the LBP algorithm uses the transpose of the sensitivity matrix due to non-existence of inverse of S as S is not a square matrix. LBP is a simple algorithm which produces approximate, but very blurred permittivity images. The LBP algorithm acts as a spatial filter with a lower cut-off frequency than that of the fundamental filter. To improve the accuracy of the LBP images, LBP is implemented using an iterative method. In the iterative method, after implementing LBP the permittivity values of K are used to back calculate inter-electrode capacitances to form a new set C_2.

$$C_2 = S.K_1 \qquad (4)$$

A set of error capacitances ΔC is then calculated which is further used to calculate error pixel values ΔK which is used to generate new set of pixel values K_2 by subtraction. Iteration is repeated by putting K_2 in (2) to calculate new set of capacitances C_3. Set of error capacitances ΔC is then calculated by subtraction of original measured capacitances from C_3 to further calculate ΔK and K_3. This iteration can be repeated as many times as desired until a satisfactorily accurate image is produced. Tikhonov Transform and Landweber Transform are algorithms to generate enhanced images without iteration. Tikhonov Transform uses equation (5) over equation (3) used in LBP to calculate permittivity distribution K.

$$K = \frac{S^T.C}{S^T.S} \qquad (5)$$

However, Tikhonov transform introduces a Tikhonov constant t along with an identity matrix I in the denominator in order to prevent the danger of division by zero if S is small. Thus equation (5) becomes,

$$K = \frac{S^T.C}{S^T.S+t.I} \qquad (6)$$

The constant t has to be chosen such that the image produced is less noisy and has higher definition. Landweber transform uses a transformation matrix Q_L defined as,

$$Q_L = V.F(W,t,N).U' \qquad (7)$$

Where V, W and U are matrices obtained from sensitivity matrix S after the process Single Value Decomposition (SVD) is applied to it. F is the SVD filter function matrix, t is the Landweber transform L and N is the number of iterations. L should be chosen such that it does not give rise to spurious artefacts around the edges of the image and it gives an image with better resolution.

RESULTS AND DISCUSSION

Voltage distribution within sensor model for various media are plotted and observed **(Figure 9)**.

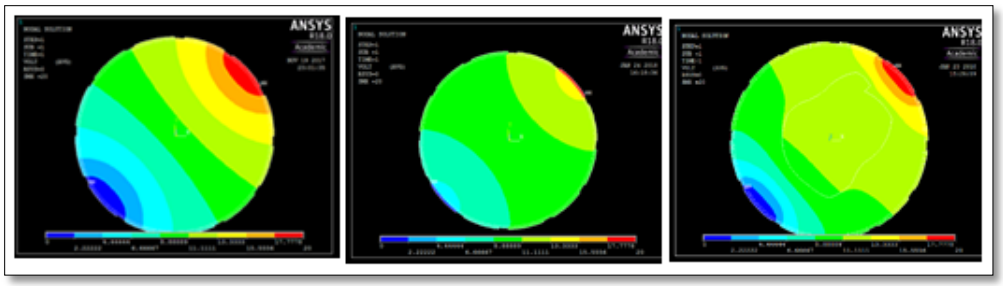

Figure 9. Voltage distributions for air, water and bone in ECT sensor.

The capacitance values obtained from ECT sensor model are plotted for electrode 1. The capacitance values are obtained for various media viz. air, water and bone. The plots for various media are compared **(Figure 10)**.

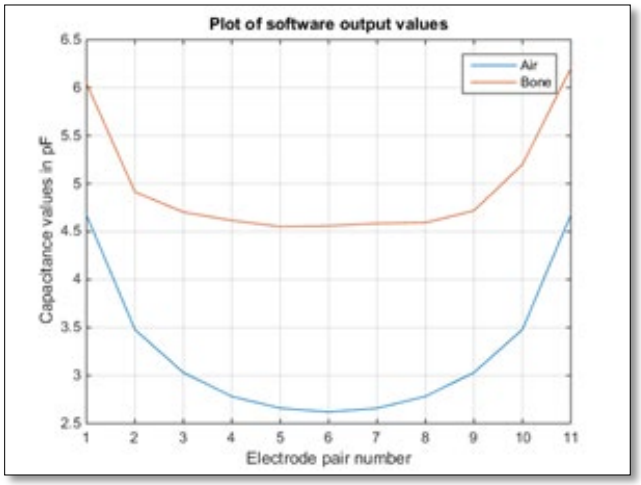

Figure 10. Plot of capacitance values for air and bone.

The output of signal converter for air and bone are plotted. The voltage values obtained from the signal converter for different media are compared and also compared with the capacitance values obtained from sensor **(Figure 11)**.

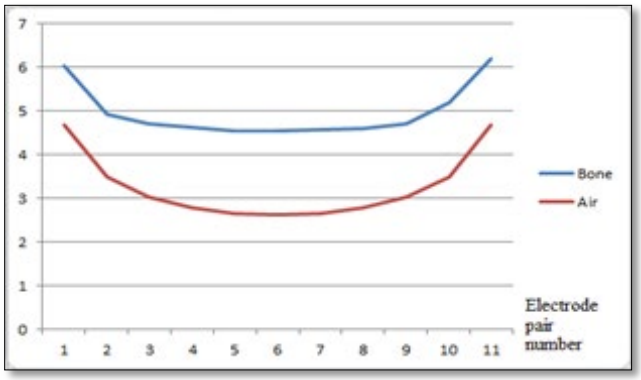

Figure 11. Plot of voltage values for air and bone.

The current values in μA obtained from the fabricated ECT sensor are plotted and compared for different media viz. air and water. They are compared with the output of sensor model as well **(Figure 12)**.

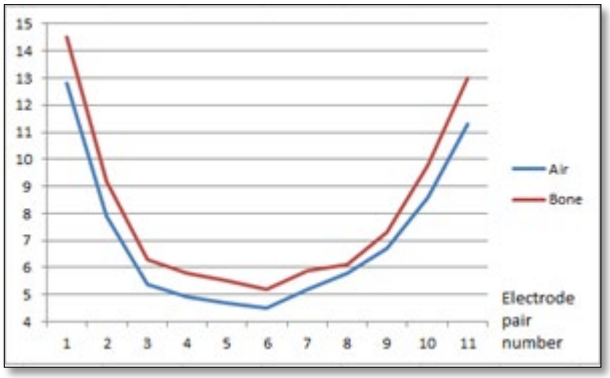

Figure 12. Plot of hardware output values for air and bone.

CONCLUSION

ECT sensor and signal converter form important parts of ECT system. It is therefore, essential to calibrate the modelled ECT sensor and implement it for bone in order to design a biomedical application based ECT system and to design a signal converter for the sensor model and implement and analyse it for different media. The voltage distribution plots of sensor model show that the voltage penetrates easily and is uniformly distributed for air with permittivity 1 while for water with permittivity 80, the voltage penetration is restricted and the distribution is non-uniform. Therefore, voltage distribution is smooth for low permittivity medium, while it is not smooth for high permittivity medium. When bone is placed within the sensor with surrounding medium as air, the distribution is smooth in air but when it encounters bone the distribution is hindered and due to permittivity variation thus non uniformity in the distribution is observed thereby indicting the effectiveness of the sensor for bone imaging. Similarly, the plots of capacitance values from the sensor model, the curve for air are the lowest, the curve for bone is in the middle and the curve for water is the highest. Air has the least permittivity; bone has second lowest permittivity and water has the highest permittivity. Therefore, we conclude that the curves are in order of their permittivity indicating that the measured capacitances are proportional to the permittivity of the medium to be imaged. The plot of current

values from the fabricated sensor shows that the curve for air is lower and smoother than that of bone similar to that of the capacitance plot while the difference between the 2 curves is small for the former plot as compared to the latter plot due to the unit of the quantities measured being different. Thus, the hardware output values plot for air and bone follow the curve as the sensor model output values plot thereby indicating that the fabricated sensor performs like the modelled sensor, approving its use for medical imaging. The signal converter circuit should convert the capacitance values to proportional voltage values which can be seen from the voltage values plot for air and bone thereby indicating the data obtained from the signal converter to be reliable to be given for further processing viz. image reconstruction.

REFERENCES

1. Ambika M, Selvakumar S (2018) Modelling, calibration and fabrication of electrical capacitance tomography sensor for bone imaging. Presented at the 3rd International Conference on Advances in Materials & Manufacturing Applications, Bangalore, India.
2. Ambika M, Selvakumar S (2018) Modeling and calibration of electrical capacitance tomography sensor for medical imaging. Biomed Pharmacol J 1: 1471-1477.
3. Manikandan K, Sathiyamoorthy S (2016) Modelling and implementation of AC electrical capacitance tomography. Circuits and Systems 7: 3818-3830.
4. Hassan MKA, Zarzour FM, Salim MS (2016) Finite element analysis of cortical bone fracture in human thigh segment. Journal of Telecommunication, Electronic and Computer Engineering 10: 135-138.
5. Manikandan K, Sathiyamoorthy S (2015) Reconstruction of image in electrical capacitance tomography. Int J Appl Eng Res 10: 30713-30724.
6. Ren Z (2015) Exploration of medical applications of electrical capacitance tomography. Ph.D. Thesis, University of Manchester.
7. Sun J, Yang W (2015) A dual-modality electrical tomography sensor for measurement of gas-oil-water stratified flows. Measurement 66: 150-160.
8. Kryszyn J, Smolik WT, Radzik B, Olszewski T, Szabatin R (2014) Switchless charge-discharge circuit for electrical capacitance tomography. Measurement Science and Technology 25.
9. Li Y, Yang W, Wu Z, Tsamakis D (2013) Gas/oil/water flow measurement by electrical capacitance tomography. Measurement Science and Technology.
10. Abraham BB, Anitha G (2012) Designing of lab view based electrical capacitance tomography system for the imaging of bones using NI ELVIS and NI USB DAQ 6009. Bonfring International Journal of Power Systems and Integrated Circuits 2: 2277-5072.
11. Zimam MA, Mohamad EJ, Rahim RA, Ling LP (2012) Sensor modeling for an electrical capacitance tomography system using comsol multiphysics. Jurnal Teknologi 55: 33-47.
12. Process Tomography Ltd. (2009) Electrical capacitance tomography system type TFLR 5000. Available at: http://www.tomography.com
13. Yan H, Liu LJ, Qiang DZ (2009) An iterative electrical capacitance image reconstruction algorithm. International Symposium on Computational Intelligence and Design.